A quantitative comparison of stimulation and post-processing thermographic inspection methods applied to aeronautical carbon fiber reinforced polymer

by R. Usamentiaga*, P. Venegas**, J. Gueredíaga**, L. Vega** and I. López**

*Department of Computer Engineering, University of Oviedo, Campus de Viesques, 33204 Gijón, Spain, *rusamentiaga@uniovi.es*
**Centro de Tecnologías Aeronáuticas (CTA), Parque Tecnológico de Álava, Juan de la Cierva 1, 01510 Miñano, Spain, pvenegas@ctaero.com

Abstract

Active thermographic inspection is a very powerful tool for many areas of science. However, there is no agreement about the proper stimulation and post-processing method for a particular material and defect type which forces technicians to carry out trial and error tests. This paper presents a comparison of three stimulation and six post-processing thermographic inspection methods applied to aeronautical carbon fiber reinforced polymer with different kind of simulated defects. The obtained results have been quantitatively assessed using the SNR metric. Conclusions provide recommendations for technicians interested in thermographic inspection of this type of material.

1. Introduction

Infrared thermography (IRT) for non-destructive testing (NDT) is a proven technology which offers reliable information about subsurface anomalies [1]. Two different approaches are employed: passive and active, the latter being more common. In active IRT an external stimulus is applied to the source of the inspected specimen causing non-stationary heat flow. The propagation of heat depends on many material properties, such as thermal conductivity or density, but also on subsurface anomalies which result in temperature differences on the surface target. This process is observed by an infrared camera which records the radiation emitted by the surface of the target at a specific wavelength range in the infrared spectrum. The acquired information is transferred to a computer for later interpretation, or post-processing. The infrared radiation emitted by the surface of the target can be converted into temperature values using the camera calibration, the properties of the material such as emissivity, and the acquisition conditions such as reflected temperature, atmospheric temperature or relative humidity.

In order to induce relevant thermal contrasts between defective and non-defective areas in the specimen under examination, an external stimulus is necessary. Many different stimulation methods can be applied. However, most of them can be classified as optical, mechanical or inductive. Optical stimulation uses light to deliver energy to the specimen. In the case of mechanical stimulation, energy is applied to the specimen by means of mechanical oscillations using, for example, an ultrasonic transducer. These stimulation methods are the most common, although inductive methods have received considerable attention recently. The applied stimulation generates heat which propagates as thermal waves from the surface through the specimen. When the thermal waves reach an anomaly they change their propagation rate, producing thermal contrast on the surface immediately above the anomaly.

Some subsurface anomalies are very subtle. Therefore, the signal levels associated to them can be lost in the thermographic data noise. In these cases the visual inspection of the acquired thermographic data does not provide positive results. One possible solution is to apply a post-processing method in order to improve the signal-to-noise content of thermographic data [2]. These methods optimise the location and visualization of defects, greatly improving the defect detection rate. Some of the most common post-processing methods are contrast analysis, Fourier transform, and Thermographic Signal Reconstruction.

No agreement has been reached among the NDT community about the proper stimulation and post-processing methods for a particular material and defect type. There are some general recommendations, but in general trial and error seems to be the preferred approach [3]. This is why survey, comparison and assessment of existing methods applied to particular cases are so important in this field; they provide recommendations and guidelines for technicians interested in NDT applied to particular cases, which greatly simplifies their work.

This paper presents a comparison of stimulation and post-processing thermographic inspection methods applied to carbon fiber reinforced polymer (CFRP). This material has many applications due to its high strength-to-weight ratio and good rigidity. CFRP is used extensively in many areas, but is particularly important in the aeronautical industry where light and strong materials are required to build the structures of the airplanes. Aircraft structural component quality control requires reliable testing procedures of all the materials involved in the construction of the structures of planes. Thus, efficient NTD of CFRP is of utmost importance in the aeronautical industry.

In this work three stimulation and six post-processing methods have been applied to the thermographic inspection of a CFRP specimen with different kinds of simulated defects. The stimulation methods are optical pulse, optical step heating and ultrasounds. Also two different amplitude presets have been used for step heating and ultrasound resulting in five different stimulation methods. The selected post-processing methods are polynomial fit, first

and second derivatives [4], phase of the Discrete Fourier Transform [5, 6], Skewness [7], and Kurtosis [8]. This means 5 stimulation methods X 6 post-processing methods. The obtained results have been quantitatively assessed for each of the 20 defects of the specimen using the SNR metric.

2. Selected excitation methods

2.1. Optical pulse

Optical pulsed thermography (OPT) is one of the most common stimulation methods. It consists of a short (pulsed) heating of the specimen for a few milliseconds. Then, the temperature decay curve is recorded with the infrared camera. The presence of defects reduces the diffusion rate resulting in thermal contrast on the surface of the specimen, immediately above the defects. Generally, the pulse is generated with flash lamps.

2.2. Step heating

Optical step heating thermography (OSHT) uses a much longer pulse than the previous stimulation method. These pulses can last more than 10 seconds. Both the temperature increase and decay are of interest. Deviations from the temperature evolution of a sound area indicate subsurface anomalies. Generally, this type of stimulation is applied using halogen lamps.

2.3. Ultrasound

Ultrasound thermography (UT) uses an ultrasonic transducer in contact with the specimen to transmit mechanical oscillations. Heat is released by friction where subsurface anomalies are located. This stimulation method has a disadvantage: it is necessary to relocate the transducer to cover the inspection area. However, it is more efficient in the inspection of cracks than optical stimulation methods.

3. Selected post-processing methods

3.1. Polynomial fit and derivatives

Polynomial fit is a common enhancing and filtering method in thermographic inspection. This method fits the temperature time history of each pixel to an n-degree polynomial as shown in Eq. (1). Then, the resulting polynomials are differentiated to produce first and second derivatives.

$$T(t) = a_n t^n + a_{n-1} t^{n-1} + \ldots + a_1 t + a_0 \tag{1}$$

In the case of pulsed thermography, the temperature time history of each pixel is previously converted to a logarithmic domain to improve the fit, as shown in Eq. (2). Then, the process is inverted using Eq. (3), resulting in a reconstructed temperature-time curve for each pixel.

$$ln\left[T(t)\right] = a_n \left\{\ln\left[t\right]\right\}^n + a_{n-1} \left\{\ln\left[t\right]\right\}^{n-1} + \ldots + a_1 \left\{\ln\left[t\right]\right\} + a_0 \tag{2}$$

$$T(t) = \exp\left(a_n \left\{\ln\left[t\right]\right\}^n + a_{n-1} \left\{\ln\left[t\right]\right\}^{n-1} + \ldots + a_1 \left\{\ln\left[t\right]\right\} + a_0\right) \tag{3}$$

Polynomial fit and differentiation are commonly called Thermographic Signal Reconstruction (TSR). However, as we do not apply all the steps of the TSR method, this paper will use the terms Fit, Fit' and Fit'' when referring to the polynomial fit and to the first and second derivatives.

Phase, Skewness and Kurtosis methods will also use the polynomial fit as a preprocessing step. That is, they will be applied to the fitted data and not to the raw data. Polynomial fit not only reduces the data, but also the noise content, which improves the results of the subsequent post-processing methods.

3.2. Phase

In order to calculate the phase of the thermographic data, the temperature time history of each pixel is transformed into the frequency domain using the Discrete Fourier Transform. This method applied to OPT is called Pulsed Phase Thermography (PPT) and combines the advantages of modulated and pulse infrared thermography.

PPT is performed with the Discrete Fourier Transform (DFT) on the temperature time history of each pixel using Eq. (4), where *i* is the imaginary number, *n* is the frequency increment, and Re_n and Im_n are the real and imaginary parts of the DFT.

$$F_n = \sum_{k=1}^{N-1} T(k) e^{\frac{2\pi i k n}{N}} = Re_n + Im_n \tag{4}$$

The phase is finally computed using Eq. (5).

$$\phi_n = \operatorname{atan}\left(\frac{Im_n}{Re_n}\right) \tag{5}$$

3.3. Skewness

Skewness of a random variable is the third standardized moment, and it measures the asymmetry in a set of statistical data. The balanced normal distribution has a skewness of zero, negative skewness means that data points are skewed to the left, and positive skewness means that data points are skewed to the right. Skewness is defined for univariate data x_1, x_2, …, x_N, as shown in Eq. (6), where μ is the mean, σ is the standard deviation, and *N* is the number of data points.

$$Skewness = \frac{\sum_{i=1}^{N}(x_i - \mu)^3}{(N-1)\sigma^3} \tag{6}$$

Skewness is applied to the temperature time history of each pixel.

3.4. Kurtosis

Kurtosis of a random variable is the fourth standardized moment. Kurstosis measures whether the data are peaked or flat. Data with high kurtosis have a distinct peak and heavy tails. On the other hand, data with low kurtosis have a flat top. Kurtosis is defined for univariate data x_1, x_2, …, x_N, as shown in Eq. (7), where μ is the mean, σ is the standard deviation, and *N* is the number of data points.

$$Kurtosis = \frac{\sum_{i=1}^{N}(x_i - \mu)^4}{(N-1)\sigma^4} \tag{7}$$

Kurtosis is applied to the temperature time history of each pixel.

4. Estimation of signal-to-noise ratio

The SNR metric is used to quantitatively assess the signal-to-noise ratio of the acquired and processed data [9]. The quantification of a defect is based on the definition of two areas: the defective area and the reference area. The defective area encloses the pixels where the defect appears in the infrared image. This area is considered the signal. The reference area, also called the sound area, is a defect-free area used to calculate the thermal contrast. This area is considered the noise.

The reference area is selected independently for each defect and must be located close to it. Thus, the reference area is known to have received the same excitation energy as the defect. This minimizes errors in SNR calculations due to non-uniform heating.

The SNR metric for a defect is calculated as shown in Eq. (8), where Def_μ is the arithmetic mean of all the pixels inside the defective area, Ref_μ is the arithmetic mean of all the pixels inside the reference area, and Ref_σ is the standard deviation of the pixels inside the reference area.

$$SNR = 20\log_{10}\left(\frac{\left|Def_\mu - Ref_\mu\right|}{Ref_\sigma}\right) \tag{8}$$

5. Experimental setup

5.1. Test piece

Fig. 1 shows the test piece used in the experiments. It is a CFRP specimen used to build aeronautical structures. As can be seen, unlike most specimens used in this type of experiments the test piece is not flat. This increases the complexity of the tests due the differences in emissivity caused by the angle of the surface with the camera. However it also makes it possible to compare the stimulation and post-processing methods in a different setup with a real piece used to build aircraft structural components. The test piece employed in the tests has several artificial defects tagged with numbers, from 1 to 20. They correspond to different types of defects, with different sizes and depths.

The specimen is made of several layers of carbon-fiber filled with epoxy, as can be seen in Fig. 2. In the thickest part, the test piece contains 16 layers, whereas in the thinnest part it contains only 7. Each layer is numbered from 1 to 16, where layer number 16 is the closest layer to the surface on which the temperature is measured. Four zones, from A to D, are also tagged in the test piece. Each zone corresponds to an area where the angle between the surface and the camera is similar.

The description of the defects can be seen in Table 1. Defects 1 to 4 are the deepest; they are located between layers 10 and 11. Defects 5 to 8 are located between layers 13 and 14, and the rest of the defects are located one layer below the surface. Most of the defects are type “void”, that is, the defect is a hole in a carbon-fiber layer. These defects have two diameters: 4 and 6 mm, and they are located in different zones of the specimen. Defects 13 to 15 are type “Flash Breaker”. In this case, these defects represent remnants of Flash Breaker tape attached to a carbon-fiber layer. Flash Breaker tape is a high grade, thick, high-temperature resistant tape used in the aerospace industry. Defects 16 to 18 are type “Separator film”, which indicates a type of defect similar to “Flash Breaker” but in this case, the remnants are standard carbon-fiber separator film.

5.2. Stimulation and acquisition

For optical pulse stimulation two flash lamps have been used in reflection mode. The flash heating system outputs a heating pulse of approximately 6 kilojoules for 1 millisecond.

In the experiments with optical step heating stimulation three halogen lamps of 1000 watts were used. The lamps were turned on for 10 seconds to heat the specimen. After the lamps were turned off, the temperature decay was recorded for another 15 seconds, making a total of 25 seconds. Both parts of the temperature time history were analyzed independently as they can contain different information. Two different configurations were used. The first one used the halogen lamps at 45% capacity. In the second configuration the halogen lamps were at 90% capacity. The heating period in both configurations was the same.

For ultrasound stimulation, the ultrasonic transducer EDE-UTVIS20-2200 was used. It has a maximum of 4000 watts of power although it was used at only 7% capacity. The ultrasonic transducer was attached to the specimen at three spots from where the waves were launched into the test piece. The experiments were recorded for 20 seconds.

All the experiments were recorded using a FLIR SC5000 camera. This camera is equipped with a cooled Indium antimonide detector which operates in the 2.5 to 5.1 μm waveband. The FLIR SC5000 produces thermal images of 320 x 256 pixels with 12 bits per pixel and a thermal sensitivity of 20 mK. Although the camera has a maximum frame rate of 383 Hz, the experiments were recorded at 50 Hz to reduce the number of acquired images.

6. Results and discussion

The results of the experiments can be seen in Table 2. The table has 8 large cells. The first row contains the first four cells, which correspond to optical step heating thermography (OSHT). The phase of the experiment where the specimen is being heated (warming-up) is treated independently from the cooling-down period. The second row corresponds to optical pulsed thermography (OPT) and ultrasound thermography (UT) in the three selected spots. The table uses a color scale in which green color indicates a good SNR, yellow is a medium SNR and red is a null SNR. The SNR metric is calculated for each defect, stimulation, and post-processing method. The SNR was only calculated when the defect was recognizable in the resulting images. Thus, the null values in the table indicate that the method was unable to identify that defect.

Some of the resulting images from the experiments can be seen in Fig. 3. Given the number of experiments it is not feasible to include all the resulting images. Thus, only those which are most interesting or which provided the best results are shown. They cover all the stimulation methods with the post-processing methods which generated better defect detection rates. As can be seen in the images, the thermal contrast of each defect has been improved independently for better visualization. However, this visualization enhancement does not affect the SNR calculation. Also, the SNR is independent of how the defects appear in the images, cooler or hotter than the surroundings (black versus white or white versus black), because the SNR assesses the same thermal contrast either way.

Results show that stimulation OSHT and OPT provided similar results, with good SNR and high defect detection rate. On the other hand, UT stimulation provided very bad results in most cases, which indicates that, for this type of defects, stimulation with ultrasound is not appropriate. When using OSHT the cooling-down phase of the experiment

shows slightly better results than the warming-up phase. Also, in OSHT 90% capacity experiments resulted in better results than 45% capacity experiments.

In terms of post-processing methods, results show that the second derivative of the polynomial fit (Fit''), Skewness (Ske), and Kurtosis (Kur) provided the best results. The second derivative of the polynomial fit with OPT made it possible to detect almost all kind of defects, although not in the same frame. Also, the resulting images, which can be seen in Fig. 3a and Fig. 3b, show a high SNR. Skewness and Kurtosis also provided very good defect detection rates but with lower SNR than Fit''. The phase of the DFT (Pha) also proved to be very effective in the cooling-down phase of one of the OSHT experiments.

In general, the second derivative of the polynomial fit combined with optical pulsed thermography are the combination of stimulation and post-processing methods which provide the best results. However, there is no single stimulation or post-processing method which maximizes SNR and defect detection rate. For example defects 1 and 3 were only detected by Skewness with OPT, and defect 17 and 18 by Skewness and Kurtosis with OSHT. Also it is important to take into account that Fit'' generates a video and not all defects are recognizable in all frames. On the other hand, Skewness and Kurtosis generate a single image where defect inspection is easier. Results shown in this paper for Phase, Skewness and Kurtosis have been obtained using the polynomial fit as a preprocessing step. Applying these post-processing methods on raw data degraded their performance considerably.

Results show a strong correlation between the depth of the defect and the SNR. The deeper the defect the lower the SNR. This is a known issue of non-destructive thermographic inspection because the detection of deeper defects requires more energy. Defects of type “Void” 9 to 12 and 19, 20, located close the surface between layers 15 and 16 have a high SNR. These defects can be clearly seen in the resulting thermographic images, even without using any post-processing methods. However, deeper defects of the same type become more difficult to detect. Defects 5 to 8 located between layers 13 and 14 can only be detected after applying post-processing methods. The combination of OPT stimulation and Fit'' provides very good results for these defects. Defects 1 to 4 located between layers 10 and 11 are hardly detected with any stimulation and post-processing methods applied. The depth of these defects could be considered as a threshold for the success of thermographic inspection. Deeper defects would probably go completely undetected.

The diameter of the defect has a slight influence in the resulting SNR. For example, the only difference between defects 9 and 11 is a 2 mm difference in diameter, defect 9 being longer. The obtained SNR for these defects is very similar, on average there is a difference of 5% when the area of defect 9 is twice the area of defect 11. However, the SNR seems to be much more influenced by the zone where the defect is located, as can be seen comparing defect 9 and 10, or 11 and 12. Defects in zone B have a much higher SNR than defects in zone D. These results indicate that the emissivity caused by the angle of the surface with the camera has a strong influence on the results. Unlike defects in zone D, the angle between the surface of defects in zone B with the camera is nearly straight, that is, this zone has a higher emissivity than zone D. This increased emissivity results in much higher SNR values in the experiments. Thus, defects with higher emissivity are easier to detect.

The detection of defects caused by remnants of covering attached to a carbon-fiber layer seems to depend on the type of covering. Defects 13 to 15 with remnants of Flash Breaker are easy to detect whereas defects 16 to 18 with remnants of standard separator film go nearly undetected. The detection key for this type of defects seems to be related to the thickness of the covering and to its thermal properties, such as thermal conductivity.

7. Conclusions

In this work three stimulation and six post-processing methods are quantitatively compared. These methods have been applied to the thermographic inspection of a real CFRP specimen used to build aircraft structural components with different kinds of simulated defects. The SNR metric has been calculated for each stimulation and post-processing method to make quantitative comparisons possible.

Results show that, in general, the second derivative of the polynomial fit combined with optical pulsed thermography are the most appropriate post-processing and stimulation methods for the detection of different types of defects in CFRP. Optical step heating stimulation also provided similar results but with longer experiments. The results show than the cooling-down phase of experiments with this type of stimulation provides slightly better results than the warming-up phase. Also, increasing the capacity of the halogen lamps improved the results. On the other hand, ultrasonic stimulation provided very bad results in most cases, which leads us to discourage technicians from using this stimulation method for this type of defects. Skewness and Kurtosis also showed very good performance for defect detection rate in both optical pulsed thermography and optical step heating thermography, making it possible to detect some defects which were hidden with other methods. These two methods used the polynomial fit as a preprocessing step, which proved to be an excellent method to reduce noise and improve the performance of any post-processing method.

Results also indicate a strong correlation between the depth of the defect and the SNR obtained. Deeper defects are harder to detect. The experiments indicate that a depth of 5 layers of carbon-fiber is a detection threshold. Deeper defects will not be detected without increasing the energy, which could damage the inspected piece. The emissivity caused by the angle of the surface with the camera also has a strong influence on the results. The best results are obtained when the surface of the defects has a nearly right angle with the camera.

The detection of defects caused by holes in a carbon-fiber layer depends mostly on the depth of the defect. However, the detection of defects caused by remnants of covering attached to a carbon-fiber layer also depends on the

type of covering. A defect caused by a thick covering with high thermal conductivity can be easily detected. However, defects caused by standard separator film could not be detected.

ACKNOWLEDGEMENTS

This work was supported by the Basque Country Regional Ministry of Industry, Innovation, Trade and Tourism under Project PREDATER for grants received from Scientific-Technological Agents integrated in the Basque Science, Technology and Innovation Network.

Also, the authors would like to acknowledge Dr. Marc Georges, Head of Laser and Non Destructive Testing Lab, Centre Spatial de Liège (CSL) - Université de Liège (Belgium), who gently supplied the specimen used in the experiments.

REFERENCES

[1] Maldague, X.P.V. 2002, "Introduction to NDT by active infrared thermography", *Materials Evaluation,* vol. 60, no. 9, pp. 1060-1073.
[2] Ibarra-Castanedo, C., González, D., Klein, M., Pilla, M., Vallerand, S. & Maldague, X. 2004, "Infrared image processing and data analysis", *Infrared Physics and Technology,* vol. 46, no. 1-2 SPEC. ISS., pp. 75-83.
[3] Ibarra-Castanedo, C., Genest, M., Guibert, S., Piau, J.-., Maldague, X.P.V. & Bendada, A. 2007, "Inspection of aerospace materials by pulsed thermography, lock-in thermography and vibrothermography: A comparative study", *Proceedings of SPIE - The International Society for Optical Engineering*.
[4] Shepard S.M., Lhota J.R., Rubadeux B.A., Wang D., Ahmed T., “Reconstruction and enhancement of active thermographic image sequences”, Optical Engineering, Vol. 42, No 5, May 2003, pp. 1337-1342.
[5] X. Maldague, F. Galmiche, A. Ziadi, Advances in pulsed phased thermography, Infrared Phys. Technol. 43 (2002) 175–181.
[6] X. Maldague, S. Marinetti, Pulse phase infrared thermography, J. Appl. Phys. 79 (5) (1996) 2694–2698.
[7] F. Madruga, C. Ibarra-Castanedo, O. Conde et al., “Automatic data processing based on the skewness statistic parameter for subsurface defect detection by active infrared thermography,” Proc. QIRT 9–Quantitative Infrared Thermography, (2008).
[8] F. J. Madruga, C. Ibarra-Castanedo, O. M. Conde et al., "Enhanced contrast detection of subsurface defects by pulsed infrared thermography based on the fourth order statistic moment, kurtosis," Proc. SPIE - Int. Soc. Opt. Eng. (USA). Thermosense XXXI, 14 April 2009.7299, 72990U (8 pp.).
[9] P. Albendea, F. J. Madruga, A. Cobo and J. M. López-Higueral, “Signal to noise ratio (SNR) comparison for pulsed thermographic data processing methods applied to welding defect detection”, QIRT 2010.

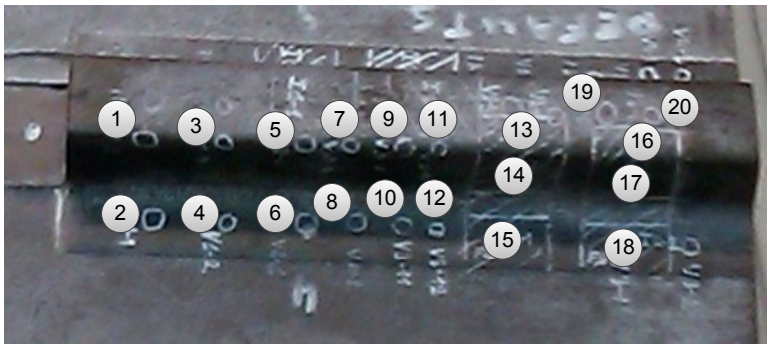

Fig. 1. *Defect map*

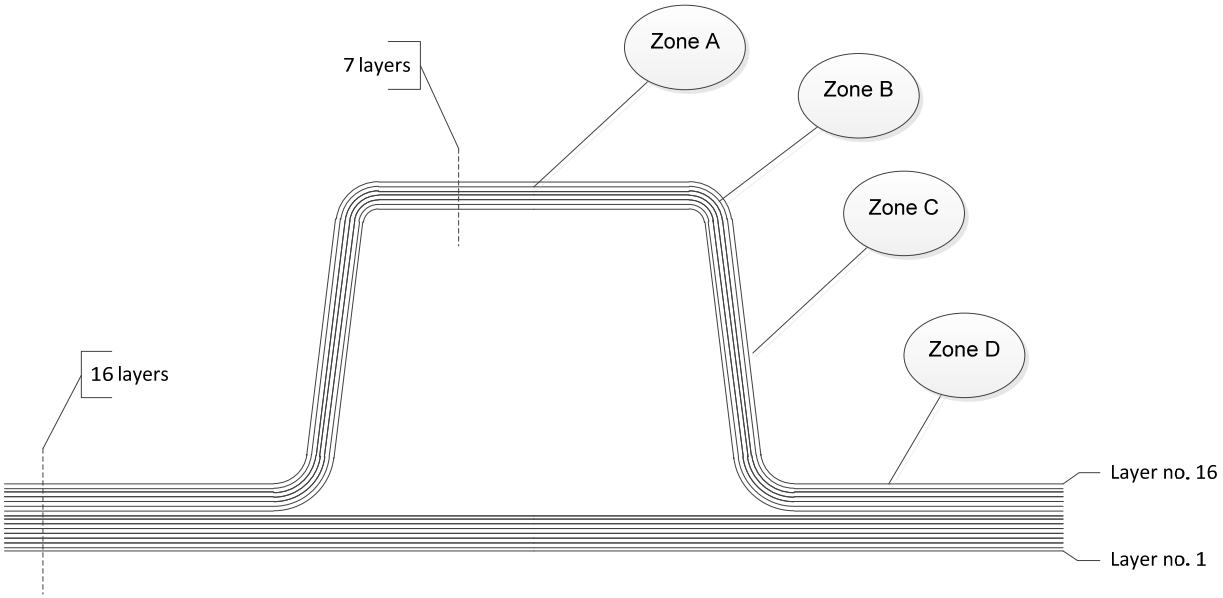

Fig. 2. *Layers of the test piece*

Table 1. *Description of the defects*

Defect No.	Type	Position	Layer No.	Diameter (mm)
1	void	B	10-11	6
2	void	D	10-11	6
3	void	B	10-11	4
4	void	D	10-11	4
5	void	B	13-14	6
6	void	D	13-14	6
7	void	B	13-14	4
8	void	D	13-14	4
9	void	B	15-16	6
10	void	D	15-16	6
11	void	B	15-16	4
12	void	D	15-16	4
13	Flash Breaker	A	15-16	
14	Flash Breaker	C	15-16	
15	Flash Breaker	D	15-16	
16	Separator film	A	15-16	
17	Separator film	C	15-16	
18	Separator film	D	15-16	
19	void	A	15-16	6
20	void	A	15-16	4

Table 2. SNR values for each defect using the selected stimulation and post-processing methods

	OSHT warming-up 45%							OSHT cooling-down 45%							OSHT warming-up 90%							OSHT cooling-down 90%						
Def.	Raw	Fit	Fit'	Fit''	Pha	Ske	Kur	Raw	Fit	Fit'	Fit''	Pha	Ske	Kur	Raw	Fit	Fit'	Fit''	Pha	Ske	Kur	Raw	Fit	Fit'	Fit''	Pha	Ske	Kur
1	0.0	0.0	0.0	0.0	0.0	0.0	0.0	0.0	0.0	0.0	0.0	0.0	0.0	0.0	0.0	0.0	0.0	0.0	0.0	0.0	0.0	0.0	0.0	0.0	0.0	0.0	0.0	0.0
2	0.0	0.0	0.0	0.0	0.0	0.0	0.0	0.0	0.0	0.0	0.0	0.0	0.0	0.0	0.0	0.0	0.0	0.0	0.0	5.2	0.0	0.0	0.0	0.0	0.0	9.4	6.4	7.8
3	0.0	0.0	0.0	0.0	0.0	0.0	0.0	0.0	0.0	0.0	0.0	0.0	0.0	0.0	0.0	0.0	0.0	0.0	3.9	0.0	0.0	0.0	0.0	0.0	0.0	0.0	0.0	0.0
4	0.0	0.0	0.0	0.0	0.0	0.0	0.0	0.0	0.0	0.0	0.0	0.0	5.1	3.6	0.0	0.0	0.0	0.0	0.0	0.0	0.0	0.0	0.0	0.0	0.0	4.4	7.3	8.0
5	0.0	0.0	0.0	9.4	0.0	0.0	6.2	0.0	0.0	10.5	9.3	0.0	0.0	0.0	0.0	0.0	4.1	14.9	8.5	11.4	16.5	0.0	0.0	11.3	9.7	16.0	0.0	0.0
6	0.0	0.0	0.0	0.0	0.0	0.0	0.0	0.0	0.0	3.6	0.0	0.0	1.6	8.6	0.0	0.0	0.0	0.0	0.0	6.3	7.0	0.0	0.0	0.0	0.0	8.9	10.9	9.1
7	0.0	0.0	0.0	5.3	0.0	0.0	8.2	0.0	0.0	9.1	8.4	0.0	0.0	0.0	0.0	0.0	5.1	9.9	5.6	8.0	15.5	0.0	0.0	9.5	8.7	10.7	0.0	0.0
8	0.0	0.0	0.0	0.0	0.0	0.0	0.0	0.0	0.0	6.3	0.0	0.0	7.5	6.6	0.0	0.0	0.0	0.0	0.0	0.0	0.0	0.0	0.0	0.0	0.0	10.2	10.3	10.5
9	16.2	17.8	25.5	29.4	25.2	22.2	24.1	9.8	8.3	26.1	25.7	16.9	13.2	14.2	24.7	28.3	27.9	27.5	21.2	17.8	31.9	12.4	14.4	28.5	27.4	18.8	25.4	24.2
10	8.9	10.9	16.3	19.7	9.7	20.3	20.4	5.4	5.9	10.3	10.9	4.4	7.1	7.6	9.1	8.9	23.3	24.7	20.9	15.9	16.9	8.2	8.1	14.4	16.8	12.2	16.9	8.3
11	20.6	21.0	19.8	23.1	23.9	18.2	25.5	10.3	12.1	21.7	21.6	15.1	11.4	11.4	22.4	24.0	23.2	23.9	21.1	13.8	27.8	10.7	12.8	27.0	24.1	13.6	25.7	25.5
12	5.5	5.8	18.6	13.7	3.2	3.1	9.7	2.3	5.4	6.4	7.6	0.0	0.0	4.1	13.3	6.3	17.1	14.5	10.5	12.6	9.4	8.3	13.9	19.6	14.0	0.0	11.9	9.3
13	6.3	9.0	13.5	16.2	8.7	5.4	12.1	4.4	0.0	18.0	13.8	0.0	0.0	15.4	11.7	7.3	19.1	16.1	17.4	10.1	16.6	4.5	3.7	17.5	18.1	13.4	0.0	0.0
14	8.1	6.4	16.8	24.2	18.2	13.3	22.7	3.5	3.6	19.7	17.8	18.6	15.1	15.4	11.3	17.3	21.5	22.7	21.8	10.5	27.2	5.4	7.0	21.8	20.9	16.8	11.3	8.5
15	8.3	7.0	9.4	16.3	11.8	19.6	18.6	11.7	10.3	17.7	15.2	7.1	7.1	5.3	15.5	17.8	18.4	21.1	20.3	18.2	19.5	13.3	8.8	15.9	17.3	6.2	6.2	6.5
16	0.0	0.0	0.0	0.0	0.0	0.0	0.0	0.0	0.0	0.0	0.0	0.0	0.0	0.0	0.0	0.0	0.0	0.0	0.0	0.0	0.0	0.0	0.0	0.0	0.0	0.0	0.0	0.0
17	0.0	0.0	0.0	0.0	0.0	0.0	0.0	0.0	0.0	0.0	0.0	0.0	6.9	7.9	0.0	0.0	0.0	0.0	0.0	0.0	0.0	0.0	0.0	0.0	0.0	0.0	9.1	10.5
18	0.0	0.0	0.0	0.0	0.0	0.0	0.0	0.0	0.0	0.0	0.0	0.0	6.8	7.9	0.0	0.0	0.0	0.0	0.0	0.0	0.0	0.0	0.0	0.0	0.0	0.0	6.8	0.0
19	14.7	16.7	21.4	17.9	14.7	8.6	18.7	14.2	12.2	14.8	14.3	20.1	21.7	17.6	17.1	15.8	21.7	21.8	15.9	24.3	23.5	17.6	16.2	16.0	19.4	26.9	24.2	21.4
20	15.4	15.8	18.3	16.9	11.1	8.2	21.3	12.0	16.0	15.3	13.6	22.9	23.5	20.1	18.5	17.5	21.9	21.6	15.6	14.6	12.5	14.2	17.0	18.1	15.5	24.0	22.8	22.0
	OPT							UT spot 1							UT spot 2							UT spot 3						
Def.	Raw	Fit	Fit'	Fit''	Pha	Ske	Kur	Raw	Fit	Fit'	Fit''	Pha	Ske	Kur	Raw	Fit	Fit'	Fit''	Pha	Ske	Kur	Raw	Fit	Fit'	Fit''	Pha	Ske	Kur
1	0.0	0.0	0.0	0.0	0.0	6.2	0.0	0	0	0	0	0	0	0	0	0	0	0	0	0	0	0	0	0	0	0	0	0
2	0.0	0.0	0.0	12.9	0.0	4.3	3.4	0	0	0	0	0	0	0	0	0	0	0	0	0	0	0	0	0	0	0	0	0
3	0.0	0.0	0.0	0.0	0.0	10.3	0.0	0	0	0	0	0	0	0	0	0	0	0	0	0	0	0	0	0	0	0	0	0
4	0.0	0.0	0.0	10.8	0.0	0.0	0.0	0	0	0	0	0	0	0	0	0	0	0	0	0	0	0	0	0	0	0	0	0
5	0.0	0.0	0.0	15.6	0.0	2.1	5.0	0	0	0	0	0	0	0	0	0	0	0	0	0	0	0	0	0	0	0	0	0
6	0.0	0.0	0.0	9.8	10.6	10.3	6.0	0	0	0	0	0	0	0	0	0	0	0	0	0	0	0	0	0	0	0	0	0
7	0.0	0.0	0.0	10.2	0.0	0.0	0.0	0	0	0	0	0	0	0	0	0	0	0	0	0	0	0	0	0	0	0	0	0
8	0.0	0.0	0.0	13.0	0.0	0.0	0.0	0	0	0	0	0	0	0	0	0	0	0	0	0	0	0	0	0	0	0	0	0
9	13.9	10.3	14.0	21.5	16.6	11.3	12.4	0	0	0	0	0	0	0	0	0	0	0	0	0	0	0	0	0	0	0	0	0
10	16.1	12.1	18.2	21.6	21.8	11.9	14.7	0	0	0	0	0	0	0	0	0	0	0	0	0	0	0	0	0	0	0	0	0
11	12.1	7.5	16.7	27.1	24.7	14.4	9.9	0	0	0	0	0	0	0	0	0	0	0	0	0	0	0	0	0	0	0	0	0
12	11.0	8.9	12.6	14.5	14.0	9.7	13.5	0	0	0	0	0	0	0	0	0	0	0	0	0	0	0	0	0	0	0	0	0
13	14.2	15.8	19.8	20.5	19.1	18.1	19.2	24	19	24	16	13	15	7.4	20	18	24	18	10	8.4	4.9	18	24	13	7.5	9.6	7.2	5.4
14	23.8	20.6	23.9	22.2	23.9	5.5	11.3	13	16	22	6.5	8.9	6.7	4.3	0	0	0	0	0	0	0	0	0	0	0	0	0	0
15	9.2	9.7	9.9	20.3	14.5	11.1	13.8	0	0	0	0	0	0	0	0	0	0	0	0	0	0	0	0	0	0	0	0	0
16	0.0	0.0	0.0	0.0	0.0	0.0	0.0	0	0	0	0	0	0	0	0	0	0	0	0	0	0	0	0	0	0	0	0	0
17	0.0	0.0	0.0	0.0	0.0	0.0	0.0	0	0	0	0	0	0	0	0	0	0	0	0	0	0	0	0	0	0	0	0	0
18	0.0	0.0	0.0	0.0	0.0	0.0	0.0	0	0	0	0	0	0	0	0	0	0	0	0	0	0	0	0	0	0	0	0	0
19	19.9	22.3	26.1	24.9	20.4	3.9	9.6	0	0	0	0	0	0	0	0	0	0	0	0	0	0	0	0	0	0	0	0	0
20	18.6	18.0	26.1	24.5	20.4	3.1	6.9	0	0	0	0	0	0	0	0	0	0	0	0	0	0	0	0	0	0	0	0	0

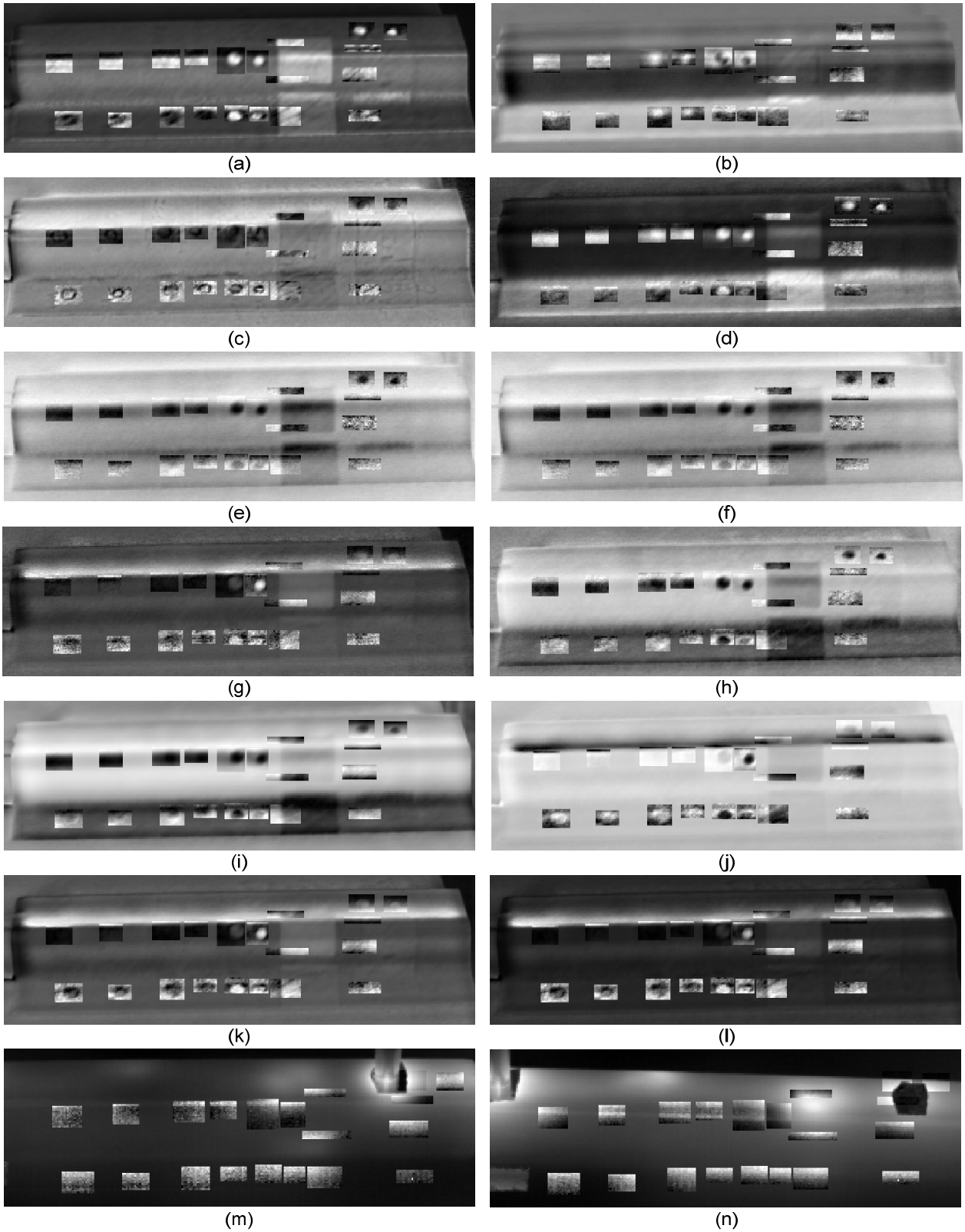

Fig. 3. *Resulting images for some of the stimulation and post-processing methods. (a), (b): OPT Fit'', (c): OPT Skewness, (d): OSHT warming-up 45% kurtosis, (e), (f): OSHT CD 45% Fit', (g): OSHT CD 45% Skewness, (h): OSHT WU 90% Phase, (i): OSHT WU 90% Skewness, (j): OSHT CD 90% Phase, (k): OSHT CD 90% Skewness, (l) OSHT CD 90% Kurtosis, (m) UT spot 1 raw, (n) UT spot 2 raw. Thermal contrast has been improved for each defect independently*